Sexually divergent cortical control of affective-autonomic integration

Tyler Wallace[1], Derek Schaeuble[1], Sebastian A. Pace, Morgan K. Schackmuth, Shane T. Hentges, Adam J. Chicco, Brent Myers

[1]Equal contribution

Biomedical Sciences, Colorado State University, Fort Collins, CO

Address for correspondence
Brent Myers, Ph.D.
Department of Biomedical Sciences
Colorado State University
1617 Campus Delivery
Fort Collins, CO 80523
brent.myers@colostate.edu

Abstract

Depression and cardiovascular disease reduce quality of life and increase mortality risk. These conditions commonly co-occur with sex-based differences in incidence and severity. However, the biological mechanisms linking the disorders are poorly understood. In the current study, we hypothesized that the infralimbic (IL) prefrontal cortex integrates depression-related behaviors with the cardiovascular burden of chronic stress. In a rodent model, we utilized optogenetics during behavior and *in vivo* physiological monitoring to examine how the IL regulates affect, social motivation, neuroendocrine-autonomic stress reactivity, and the cardiac consequences of chronic stress. Our results indicate that IL glutamate neurons increase socio-motivational behaviors specifically in males. IL activation also reduced endocrine and cardiovascular stress responses in males, while increasing reactivity in females. Moreover, prior IL stimulation protected males from subsequent chronic stress-induced sympatho-vagal imbalance and cardiac hypertrophy. Our findings suggest that cortical regulation of behavior, physiological stress responses, and cardiovascular outcomes fundamentally differ between sexes.

Keywords: infralimbic cortex, social motivation, corticosterone, chronic stress, ventricular hypertrophy

Introduction

Major depressive disorder (MDD) and cardio-metabolic conditions including hypertension, glucose intolerance, and heart failure significantly contribute to global disease burden. Epidemiological evidence implicates life stressors as a risk factor for both MDD and cardiovascular disease (CVD) (Binder and Nemeroff, 2010; Grippo and Johnson, 2009; Myers et al., 2014b; Sgoifo et al., 2015). Furthermore, sex differences in the incidence of MDD, CVD, and MDD-CVD co-morbidity suggest that sex-specific factors contribute to outcomes (Goldstein et al., 2019). However, the biological basis for stress effects on health, particularly the integration of affective and physiological systems, is poorly understood. Human brain imaging studies indicate that ventral medial prefrontal cortex (vmPFC) activity associates with sadness and blood pressure reactivity, suggesting that top-down cortical control may integrate diverse aspects of mood and systemic physiology.

The vmPFC is involved in numerous cognitive and emotional processes (McKlveen et al., 2015; Myers-Schulz and Koenigs, 2012; Wood and Grafman, 2003). A subregion of the vmPFC, the subgenual cingulate cortex (BA25), is activated by sadness-provoking stimuli, responds to social isolation, and has reduced volume in MDD patients (Beckmann et al., 2009; Liotti et al., 2000; Vijayakumar et al., 2017). BA25 is also targeted for deep brain stimulation in patients with treatment-resistant depression, where larger volumes predict better treatment outcomes (Mayberg et al., 2005; Sankar et al., 2019). Subgenual regions of vmPFC have also been identified as components of a central autonomic network monitoring visceral functions (Beissner et al., 2013; Gianaros and Sheu, 2009; Gianaros and Wager, 2015; Myers, 2016;

Shoemaker et al., 2016). The rodent homolog of BA25, the infralimbic cortex (IL) (Öngür et al., 2003; Uylings et al., 2003; Vertes, 2004), innervates limbic and stress-regulatory nuclei including the amygdala, thalamus, and hypothalamus (Gabbott et al., 2005; Myers et al., 2016, 2014a; Wood et al., 2018). Additionally, IL stimulation reduces passive coping and increases pyramidal neuron spine density in male rodents (Caballero et al., 2019; Fuchikami et al., 2015; Selimbeyoglu et al., 2017; van Holstein and Floresco, 2019). Moreover, knockdown of IL glutamatergic output exacerbates chronic stress effects on hypothalamic-pituitary-adrenal (HPA) axis reactivity and vascular function (Myers et al., 2017; Schaeuble et al., 2019). However, the potential sex-specific roles of IL activity to integrate socio-motivational behaviors with physiological stress reactivity and the cardiac outcomes of chronic stress remain to be determined.

In the current study, channelrhodopsin-2 (ChR2) was expressed under the calcium/calmodulin-dependent protein kinase type II α (CaMKIIα) promoter in the IL to permit optogenetic activation of IL pyramidal neurons in both male and female rats (Wood et al., 2018). This approach was combined with measures of place preference and social behavior to examine affective valence and sociability. Behavioral assessment was followed by measures of physiological stress reactivity, including radiotelemetry and echocardiography over the course of chronic variable stress (CVS). Ultimately, these findings identify the IL as an affective-autonomic integrator that links motivation and stress responding divergently in males and females.

Methods

Animals

Age-matched adult male and female Sprague-Dawley rats were obtained from Envigo (Denver, CO) with male rat weight ranging from 250-300 g and female from 150-200 g. After stereotaxic surgery, rats were housed individually in shoebox cages with cardboard tubes for enrichment in a temperature- and humidity-controlled room with a 12-hour light-dark cycle (lights on at 07:00h, off at 19:00h) and food and water *ad libitum*. All procedures and protocols were approved by the Colorado State University Institutional Animal Care and Use Committee (protocol: 16-6871A) and complied with the National Institutes of Health Guidelines for the Care and Use of Laboratory Animals. Signs of poor health and/or weight loss ≥ 20% of pre-surgical weight were *a priori* exclusion criteria. These criteria were not met by any animals in the current experiments; however, animals were removed from experimentation if fiber optic or radiotelemetry devices failed.

Microinjections

Rats were anesthetized with isoflurane (1-5%) followed by analgesic (0.6 mg/kg buprenorphine-SR, subcutaneous) and antibiotic (5 mg/kg gentamicin, intramuscular) administration. Rats received bilateral microinjections (0.75-2 μL) of adeno-associated virus (AAV) into the IL (males: 2.7 mm anterior to bregma, 0.6 mm lateral to midline, and 4.2 mm ventral from dura, females: 2.3 mm anterior to bregma, 0.5 mm lateral to midline, and 4 mm ventral from dura). AAV5-packaged constructs (University of North Carolina Vector Core, Chapel Hill, NC) either expressed yellow fluorescent protein

(YFP) or ChR2 conjugated to YFP under the CaMKIIα promoter to achieve pyramidal cell-predominant expression (Wood et al., 2018). All micinjections were carried out with a 25-gauge, 2-μL microsyringe (Hamilton, Reno, NV) using a microinjection unit (Kopf, Tujunga, CA) at a rate of 5 minutes/μL. The needle was left in place for 5 minutes before and after injections to reduce tissue damage and allow diffusion. Skin was closed with wound clips that were removed 2 weeks after injections and animals were allowed at least 6 weeks for recovery and ChR2 expression.

Electrophysiology

Adult male rats (n = 8) were injected with AAV constructs as described above and, after 8-12 weeks, exposed to 5% isoflurane prior to decapitation and brain removal. As previously described (Rau and Hentges, 2017), brains and sections were collected in ice-cold artificial CSF (aCSF) consisting of the following (in mM): 126 NaCl, 2.5 KCl, 1.2 $MgCl_2 \Lambda 6H_2O$, 2.4 $CaCl_2 \Lambda 2H_2O$, 1.2 NaH_2PO_4, 11.1 glucose, and 21.4 $NaHCO_3$, bubbled with 95% O_2 and 5% CO_2. Coronal slices containing the IL were cut at a thickness of 240 μm using a model VT1200S vibratome (Leica Microsystems, Buffalo Grove, IL). After resting 1 hr at 37°C in aCSF, slices were transferred to the recording chamber and perfused with oxygenated 37° C aCSF at a 2 ml/min flow rate. For whole-cell recordings, the internal recording solution contained the following (in mM): KCL 57.5, K-methyl sulfate 57.5, NaCl 20, $MgCl_2$ 1.5, HEPES 5; EGTA 0.1; ATP 2; GTP 0.5, and phosphocreatine 10. The pH was adjusted to 7.3. Recording electrodes had a resistance of 2 – 4 MΩ when filled with this solution. IL pyramidal neurons were identified for recording based on the expression of ChR2-YFP under the control of

CaMKIIα. Whole-cell patch-clamp recordings were acquired in voltage-clamp at a holding potential of -60 mV using an Axopatch 200B Amplifier (Molecular Devices, San Jose, CA). Current-clamp recordings were acquired while holding current at 0 pA. Electrophysiological data were collected and analyzed using Axograph X software on a Mac OS X operating system (Apple, Cupertino, CA). Light activation of IL neurons expressing ChR2 was triggered via a 5 ms 470 nm LED (Thorlabs, Newton, NJ) light pulse driven by a LEDD1B driver (Thorlabs, Newton, NJ) triggered through the TTL output on an ITC-18 computer interface board (HEKA Instruments, Holliston, MA). Current-clamp experiments utilized 5, 10, and 20 Hz stimulation frequencies for 5 min bouts. Recordings were excluded if access resistance exceeded 10 Ω during recording.

Radiotelemetry implantation

A subset of rats was instrumented with ECG-enabled radiotelemetry transmitters (HD-S11 F0, Data Sciences International, St. Paul, MN) as previously described (Flak et al., 2011; Goodson et al., 2017; Schaeuble et al., 2019). Briefly, rats were anesthetized with inhaled isoflurane anesthesia (1-5%) and given a subcutaneous injection of analgesic (0.6 mg/kg Buprenorphine-SR) and an intramuscular injection of antibiotic (5 mg/kg gentamicin). The descending aorta was exposed via an abdominal incision, allowing implantation of a catheter extending from the transmitter. The catheter was secured with tissue adhesive (Vetbond; 3M Animal Care Products, St. Paul, MN) applied over a cellulose patch. ECG leads were passed through abdominal musculature and sutured subcutaneously above the rib cage and pectoral muscles. The transmitter body was then sutured to the abdominal musculature, followed by closure of the

abdominal musculature and skin with suture and wound clips, respectively. Rats then recovered for 2 weeks before wound clips were removed.

Fiber optic cannulas

Rats were anesthetized (isoflurane 1-5%) and bilateral fiber-optic cannulas (flat tip 400/430 μm, NA = 0.66, 1.1 mm pitch with 4.5 mm protrusion for males and 4.2 mm protrusion for females; Doric Lenses, Québec, Canada) were aligned with the IL injection sites and lowered into place approximately 1 mm dorsal to the injection. Cannulas were secured to the skull with metal screws (Plastics One) and dental cement (Stoelting, Wood Dale, IL). Skin was sutured and rats were given a subcutaneous injection of analgesic (0.6 mg/kg Buprenorphine-SR) and an intramuscular injection of antibiotic (5 mg/kg gentamicin). Following 1 week of recovery, rats were handled daily and acclimated to the stimulation procedure for another week before experiments began. Rat handling and cannula habituation continued daily throughout experiments.

Optogenetic stimulation

Light pulses (1 mW, 5 ms pulses, 10 or 20 Hz) were delivered through a fiber-optic patch cord (240 μm core diameter, NA = 0.63; Doric Lenses) connected to a 473 nm LED driver (Doric Lenses). Optic power was measured with a photodiode sensor (PM160, Thorlabs Inc, Newton, NJ) at the cannula fiber tip. Rats received a single 30-minute session of stimulation (1 min on/1 min off) in their homecage during habituation the week prior to experimentation.

Estrous cycle cytology

All female rats went through experiment 3 simultaneously, housed in the same room and randomly cycling. Immediately following acute measures of behavior and/or physiology, vaginal cytology was examined to approximate the estrous cycle stage. A damp (deionized water) cotton swab was used to collect cells from the vaginal canal and place them onto a glass slide. When dried, slides were viewed under a 10x objective light microscope by a minimum of two blind observers and were categorized as proestrus, estrus, metestrus, or diestrus (Cora et al., 2015; Smith et al.; Solomon et al., 2015).

Real-time place preference

The real-time place preference (RTPP) assay was used to assess the valence of IL stimulation (Bimpisidis et al., 2020; Stamatakis and Stuber, 2012). Cannulas were connected to LEDs for light delivery and rats placed in a custom-made fiberglass arena with two chambers connected by a corridor (chambers: 15 x 15'', corridor: 8 x 6'', 15'' deep). Rats explored the arena for 10 minutes on two consecutive days. The first day was a habituation day and no stimulation was delivered on either side. On the second day, rats received LED-generated 465 nm light pulses upon entry to the assigned stimulation side. Trials were recorded by a camera mounted above the arena and animal position was tracked by Ethovision software (Noldus Information Technologies) for automated optic hardware control. Stimulation side assignment was counterbalanced and animal testing was randomized. The time rats spent in the

stimulation side was divided by the total time and multiplied by 100 to generate a percentage of time spent in the stimulation side.

Social behavior

A modified version of the 3-chambered social behavior assay was used to accommodate optic patch cords (Felix-Ortiz and Tye, 2014; Moy et al., 2004). To examine social interaction, each rat was connected to a patch cord and placed in a black rectangular fiberglass arena (36 x 23'', 15.8'' deep). Initially, the arena was empty and experimental rats were allowed to explore for 5 minutes without optic stimulation. The experimental rat was then returned to their home cage while an empty enclosure (ventilated with small round openings) was placed on one side of the arena, defined as the object, and an identical enclosure containing an age- and sex-matched conspecific was placed on the other side of the arena, defined as the social cage. The experimental rat was then placed in the middle of the arena and allowed to explore freely for 10 minutes with 5 ms pulsatile stimulation delivered throughout to quantify social motivation. The experimental rat was then placed again into its home cage while the empty enclosure was replaced with a new enclosure containing a novel age- and sex-matched conspecific. The experimental rat freely explored for 10 minutes while receiving optic stimulation to assess social novelty preference. Behavior was recorded with an overhead camera and interactions were defined as nose pokes onto cages and scored by a treatment-blinded observer. The duration of interactions was divided by the total time of each interaction period and multiplied by 100 to give a percent interaction

value. Sides for object cage, social cage, and novel cage were counterbalanced and animal order randomized.

Novel environment

Rats with radiotelemetry implants were exposed to a 30-minute novel environment stressor to assess acute cardiovascular reactivity. Rats were connected to fiber-optic patch cords and placed into a brightly-lit semi-transparent arena. Radiotelemetry receiver pads (Data Sciences International, St. Paul, MN) were arrayed under the arena with 10 Hz optic stimulation during the stressor to record hemodynamics and activity in 1-minute bins. Heart rate (HR), mean arterial pressure (MAP), systolic arterial pressure (SAP), and diastolic arterial pressure (DAP) were collected and analyzed with Ponemah software (Version:6.4x Data Sciences International).

Restraint stress

Restraint was used to examine neuroendocrine responses to acute stress. Rats were placed in plastic film decapicones (Braintree Scientific, Braintree, MA) and connected to fiber-optic patch cords for optic stimulation throughout the 30-minute restraint. Blood samples (approximately 250 μL) were collected by tail clip at the initiation of restraint with additional samples taken 15 and 30 min after (Vahl et al., 2005). At the conclusion of restraint, patch cords were disconnected and rats returned to their homecage with recovery blood samples collected at 60 and 90 min after the initiation of restraint. Blood glucose was determined with Contour Next EZ glucometers

(Bayer, Parsippany, NJ) and 2 independent readings for each time point were averaged. Blood samples were centrifuged at 3000 X g for 15 minutes at 4° C and plasma was stored at –20° C until radioimmunoassay (RIA). Plasma corticosterone levels were measured with an ^{125}I RIA kit (MP Biomedicals, Orangeburg, NY) as previously described (Myers et al., 2017). All samples for each sex were run in duplicate and all time points were run in the same assay. RIA intra-assay coefficient of variation was 8.6% and interassay 13.6%.

Chronic variable stress

Chronic variable stress was comprised of twice daily (AM and PM) repeated and unpredictable stressors presented in a randomized manner including: exposure to a brightly-lit open field (28.5 x 18'' 13'' deep, 1 hour), cold room (4° C, 1 hour), cage tilt (45°, 1 hour), forced swim (23° to 27° C, 10 minutes), predator odor (fox or coyote urine, 1 hour), restraint (1 hour), and shaker stress (100 rpm, 1 hour). Additionally, overnight stressors were variably included, comprised of damp bedding (400 mL water) and overnight light. During the 2 weeks of CVS, rats were weighed every 3-4 days to monitor body weight.

Spectral analysis of heart rate variability

Throughout CVS, resting homecage recordings of heart rate variability (HRV) were collected and analyzed using Ponemah software (Version:6.4x Data Sciences International, St. Paul, MN). Using guidelines for heart rate variance (Electrophysiology, 1996) occurring as a function of frequency, low (LF) and high frequency (HF)

components were collected during two-hour periods in the AM and PM and averaged within treatment groups. Recordings were sampled at least one hour after stressors and did not follow overnight stressors, swim, or restraint. Spectral analysis is used to measure autonomic balance as LF predominantly represents sympathetic and HF predominantly parasympathetic contributions to HRV (Electrophysiology, 1996; Sgoifo et al., 2015). Accordingly, LF/HF represents net cardiac sympathetic drive.

Echocardiography

Left ventricle structure and function were assessed before and after CVS via echocardiography. In preparation, rats were anesthetized with inhaled isoflurane (5% induction, 2% maintenance), connected to fiber optic patch cord, and shaved over the ventral thorax. A 12-mHz pediatric transducer connected to a Phillips XD11 ultrasound system was used to image the heart in transverse (parasternal short axis) and 4-chamber angles. M-mode echocardiograms were utilized to measure left ventricular end-systolic and end-diastolic chamber dimensions and anterior/posterior wall thickness (Chicco et al., 2008; Le et al., 2014). Once the measurements were taken for a rat, optics were turned on and a second exam was conducted to investigate acute stimulation-induced changes. Total exam time for each trial was approximately 5 minutes.

Tissue collection

Rats were given an overdose of sodium pentobarbital and perfused transcardially with 0.9% saline followed by 4.0% paraformaldehyde in 0.1 M PBS.

Brains were removed and post-fixed in 4.0% paraformaldehyde for 24 h at room temperature, followed by storage in 30% sucrose in PBS at 4 °C. Coronal sections were made on a freezing microtome at 30 μm thickness and then stored in cryoprotectant solution at −20 °C until processing. A subset of rats received optogenetic stimulation prior to tissue collection. Rats were tethered to a fiber optic patch cord and received 5 minutes of optic stimulation followed by 90 minutes of recovery for immediate-early gene (c-Fos) expression prior to euthanasia, as described above (Wood et al., 2018).

Immunohistochemistry and microscopy

For fluorescent labeling of c-Fos, coronal brain sections were removed from cryoprotectant and rinsed in PBS (5 x 5 min) at room temperature. Sections were then placed in blocking solution (PBS, 0.1% bovine serum albumin, and 0.2% Triton X-100) for 1 hour. Next, sections were incubated overnight in rabbit anti-c-Fos primary antibody (1:200 in blocking solution, Cell Signaling Technologies, Ab #2250). Following overnight incubation in primary antibody, sections were rinsed in PBS (5 x 5 min) and incubated in donkey anti-rabbit Cy5 secondary (1:1000 in PBS, Jackson ImmunoResearch, AB_2340607) for 1 hour. The tissue was then washed (5 x 5 min in PBS), mounted with polyvinyl medium, and cover slipped for imaging. To determine injection placement, YFP was imaged with a Zeiss Axio Imager Z2 microscope using the 10x objective, while YFP and c-Fos fluorescence were acquired as tiled 20x objective images.

Experimental Design

Timelines for *in vivo* experiments are outlined in figure 1. Experiment 1 was comprised of 2 cohorts of male rats (n = 13-14 each) to yield 10 YFP and 17 ChR2. For this experiment, real-time place preference and social behavior were assessed prior to restraint stress with 20 Hz used for all stimulation. Experiment 2 consisted of 3 cohorts of male rats (n = 7-8 each) for a total of 12 YFP and 10 ChR2. A subset of these rats was equipped with radiotelemetry transmitters (YFP n = 7, ChR2 n = 8) and all underwent real-time place preference and social behavior prior to novel environment with 10 Hz stimulation. Afterward, rats in experiment 2 underwent echocardiography before and after CVS. Experiment 3 was designed as a single cohort of female rats (n = 29) with 12 YFP and 17 ChR2. A subset of these rats was equipped with radiotelemeters (YFP n = 7, ChR2 n = 8). Real-time place preference and social motivation were followed by novel environment and restraint with 10 Hz stimulation for all measures. Female rats also underwent echocardiography before and after CVS.

Data analysis

Data are expressed as mean ± standard error of the mean. Data were analyzed using Prism 8 (GraphPad, San Diego, CA), with statistical significance set at $p < 0.05$ for rejection of null hypotheses. RTPP stimulation preference was assessed via repeated measure two-way analysis of variance (ANOVA) with virus and day (repeated) as factors. In the case of significant main or interaction effects, Sidak's multiple comparisons were run to determine group differences. Social motivation and novelty preference were assessed with unpaired t-tests to compare virus groups within social,

object, novel rat, or familiar rat interactions. Total distance traveled during RTPP and social interaction was assessed with unpaired t-tests comparing virus groups. Stress responses over time (corticosterone, glucose, HR, MAP, SAP, DAP, and HRV spectra) were analyzed using mixed-effects analysis with virus and time (repeated) as factors, followed by Fisher's post-hoc if significant main or interaction effects were present. Mean activity during novel environment was assessed with Mann-Whitney U non-parametric test comparing virus groups. Fractional shortening and ventricular structure were assessed with paired Wilcoxon signed-rank tests comparing pre- and post-CVS or optic status within virus groups.

Results

Validation and design

AAV viral vectors were targeted to the IL for expression of membrane-targeted ChR2-YFP or cytosolic YFP under the pyramidal neuron promoter, CaMKIIα. Fiber optic cannulas implanted in the IL permitted selective stimulation of IL glutamatergic neurons, as previously reported (Fuchikami et al., 2015; Wood et al., 2018). In female rats, c-Fos labeling verified *in vivo* neural activation in response to light-stimulation (10 Hz, 5 ms, 5 min) (**Fig. 1A**). Whole-cell patch-clamp recordings in slice demonstrated light-evoked depolarizing current in male IL neurons expressing ChR2 (**Fig. 1B**). Further, 10 Hz stimulation led to high-fidelity action potential generation. 20-Hz light pulses induced action potential firing, as well as increased resting membrane potential (**Fig. 1C**). These results, combined with our previous studies quantifying a 4.5-fold increase in immediate-early gene expression after 20 Hz stimulation (Wood et al., 2018), suggest that both 10 Hz and 20 Hz stimulation activate IL CaMKIIα-positive neurons. Although, 10 Hz stimulation is in line with the reported 4-10 Hz intrinsic firing rate of IL pyramidal neurons (Homayoun and Moghaddam, 2007; Ji and Neugebauer, 2012). The experimental design (**Fig. 1D**) is detailed in the methods. Male and female rats received optogenetic stimulation during behavioral and physiological measures in separate experiments. At the conclusion of all experiments, the placement of viral injections and fiber optics was determined. Only animals with cannula placement verified to be within or immediately dorsal to the IL were included in analyses (**Fig. 1E**).

Real-time place preference

RTPP was used to examine the affective valence of stimulating IL glutamatergic neurons. Group mean heat maps illustrate time spent in the stimulation versus non-stimulation chambers (**Fig. 2A**). Male rats showed a preference for the stimulation chamber (**Fig. 2B**) with 20 Hz (repeated-measures 2-way ANOVA: stimulation x ChR2 $F_{(1, 23)} = 15.04$, $p < 0.001$) and 10 Hz stimulation (repeated-measures 2-way ANOVA: stimulation $F_{(1, 20)} = 6.03$, $p < 0.05$, ChR2 $F_{(1, 20)} = 9.04$, $p < 0.01$, stimulation x ChR2 $F_{(1, 20)} = 6.427$, $p < 0.05$). Specifically, Sidak's *post hoc* indicated a preference for the 20 Hz and 10 Hz stimulation chambers compared to habituation day in the ChR2 groups (n = 10-15, $p < 0.01$). Both ChR2 groups also preferred the stimulation chamber relative to YFP animals on the stimulation day (n = 10-12, $p < 0.01$). In contrast, female rats demonstrated no preference or aversion for the chamber paired with IL stimulation (n = 11-13/group, repeated-measures 2-way ANOVA: stimulation $F_{(1, 22)} = 5.79$, $p < 0.05$, stimulation x ChR2 $F_{(1, 22)} = 0.005$ $p = 0.943$). Additionally, IL stimulation did not affect general locomotor activity in either sex (**Fig. 2C**). Together, these findings indicate that the activity of male IL glutamatergic neurons has a positive affective valance as animals were motivated to seek out the stimulation. However, this cell group does not appear to modify affective state in females.

Social behavior

The three-chamber social interaction assay was used to determine the influence of IL glutamatergic neurons on sociability. During the social motivation test (**Fig. 3A**), there was no difference in social interactions with 20 Hz stimulation in males (n = 9-

10/group, unpaired t-test: ChR2 vs YFP $t_{(17)} = 0.77$, $p = 0.452$). However, 10 Hz stimulation in males increased social interactions (**Fig. 3B**; n = 10-12/group, unpaired t-test: ChR2 vs YFP $t_{(18)} = 3.00$, $p < 0.01$). In contrast, 10 Hz stimulation in females did not impact social interaction (n = 12-16/group, unpaired t-tests: ChR2 vs YFP $t_{(24)} = 1.01$, $p = 0.321$). Furthermore, neither male nor female IL stimulation affected preference for novel vs. familiar interactors (**Table 1**). Overall, these results indicate that IL glutamatergic activity increases male social motivation in a frequency-dependent manner; however, this cell population does not alter female social motivation.

Endocrine reactivity

To study the effect of stimulating IL pyramidal neurons on neuroendocrine responses, blood glucose and plasma corticosterone were monitored during restraint stress. In males, optic stimulation decreased corticosterone (n = 10-17/group, mixed-effects: time $F_{(4,81)} = 139.4$, $p < 0.0001$, ChR2 $F_{(1,25)} = 8.93$, $p < 0.01$) at the 30-minute timepoint (**Fig. 4A**; $p < 0.01$). Additionally, corticosterone was decreased post-stimulation in the ChR2 group during stress recovery (90 min; $p < 0.05$). Stimulation also decreased blood glucose (mixed-effects: time $F_{(4,90)} = 62.86$, $p < 0.0001$, time x ChR2 $F_{(4,90)} = 3.43$, $p < 0.05$) in male rats during restraint (**Fig. 4B**; 15 min, $p < 0.01$; 30 min, $p < 0.05$). In contrast, stimulation did not alter plasma corticosterone in female rats (**Fig. 4C**; n = 10-17/group, mixed-effects: time $F_{(4,93)} = 62.94$, $p < 0.0001$) with effects of time limited to within treatment. Additionally, stimulation increased glucose responses to stress in female rats (n = 10-17/group, mixed effects: time $F_{(4,90)} = 24.96$, $p < 0.0001$) specifically at the 15-min timepoint (**Fig. 4D**; $p < 0.05$). Collectively, these results

suggest that IL activity in males reduces HPA axis activation as well as glucose mobilization. In females, IL activity does not appear to alter HPA axis response to stress. However, IL stimulation in females increases glucose, possibly through sympathetic mobilization of epinephrine and/or glucagon.

Cardiovascular reactivity

Exposure to a brightly-lit novel environment was used as a psychogenic stimulus to examine IL glutamatergic effects on cardiovascular reactivity. Over the course of the stressor, there were no differences in activity between male YFP (n = 7) and ChR2 (n = 8) rats (**Fig. 5A**; Mann-Whitney: U = 407, $p = 0.53$). In terms of hemodynamic responses, stimulation decreased HR reactivity in male ChR2 rats (mixed-effects: time $F_{(30,280)} = 19.61$, $p < 0.0001$, time x ChR2 $F(_{30,280}) = 2.06$, $p < 0.01$), an interaction present at the 8-minute timepoint (**Fig. 5B**; $p < 0.05$). After the first minute of stimulation, arterial pressures including mean (mixed-effects: time $F_{(30,172)} = 25.99$, $p < 0.0001$, time x ChR2 $F(30,172) = 1.86$, $p < 0.01$), systolic (mixed-effects: time $F_{(30,213)} = 27.61$, $p < 0.0001$), and diastolic (mixed-effects: time $F_{(30,189)} = 20.56$, $p < 0.0001$, ChR2 $F_{(1,12)} = 8.05$, $p < 0.05$, time x ChR2 $F_{(30,189)} = 2.38$, $p < 0.01$) were decreased in male ChR2 rats. Post-hoc analysis indicated these effects were present across numerous timepoints (**Fig. 5C-E**; 7-28 minutes; $p < 0.05$). In contrast, stimulation increased MAP and DAP in minute 1 ($p < 0.05$). For females, there was no effect of ChR2 on activity in the novel environment (**Fig. 5F**; n = 7-8, Mann-Whitney: ChR2 vs YFP U = 352, $p = 0.15$). However, IL activation increased female HR responses (mixed effects: time $F_{(30,390)} = 25.83$, $p < 0.0001$) early in the stressor (**Fig. 5G**; 1-9 min; $p < 0.05$) as well as

at 25 min ($p < 0.05$). Mixed effects analysis of arterial pressure found main effects of time for MAP (**Fig. 5H**; time $F_{(30,390)} = 31.96$, $p < 0.0001$) and SAP (**Fig. 5I**; time $F_{(30,390)} = 35.01$, $p < 0.0001$) without virus-specific effects. Taken together, these results indicate activation of male IL glutamate neurons decreases HR and arterial pressure responses to psychological stress. In contrast, activation in females increases HR.

Effects of chronic stress on cardiac function

Resting homecage LF/HF of HRV was recorded via radiotelemetry to assess how prior optic stimulation affected circadian autonomic balance and net cardiac sympathetic drive during CVS. In the absence of ongoing stimulation, ChR2 (n = 8) males had lower LF/HF than YFP (n = 7) rats (**Fig. 6A**; mixed-effects: time $F_{(5,62)} = 4.45$, $p < 0.01$, ChR2 $F_{(1,13)} = 5.33$, $p < 0.05$). In the AM the day prior to CVS, ChR2 males had lower baseline LF/HF ($p < 0.05$) leading to decreased sympathetic drive the morning of CVS day 14 ($p < 0.05$). In females, there were circadian effects on LF/HF (**Fig. 6B**; n = 5-6/group, mixed-effects: time $F_{(5,45)} = 5.98$, $p < 0.01$) but no differences due to virus (mixed-effects: ChR2 $F_{(1,9)} = 1.28$, $p > 0.05$).

Left ventricle echocardiography was performed before and after CVS to examine the *in vivo* cardiac consequences of chronic stress and the effects of IL stimulation on cardiac contractility. Fractional shortening (FS) was measured as the portion of diastolic dimension lost in systole. In male rats treated with YFP (n = 8), CVS increased FS (**Fig. 6C**; Wilcoxon: Post vs Pre W = 30.0, $p < 0.05$). In contrast, there was no effect of CVS on FS in ChR2 (n = 8) males (Wilcoxon: Post vs Pre W = -4.0, $p = 0.84$). To determine whether post-CVS FS was affected by acute stimulation, measurements were taken

with optics off and then on (**Fig. 6D**). Here, a cohort of males showed no effect of acute optic status on FS (n = 3-4/group, Wilcoxon: YFP On vs Off W = 4.0, $p = 0.13$; ChR2 On vs Off W = 2.0, $p = 0.75$). In females there was no effect of CVS on FS (**Fig. 6E**; n = 10, YFP Post vs Pre W = -21.0, $p = 0.25$; n = 17, ChR2 Post vs Pre W = 53.0, $p = 0.07$). However, optic stimulation increased post-CVS FS in ChR2 animals (**Fig. 6F**; Wilcoxon: On vs Off W = 87.0, $p < 0.01$). In aggregate, these findings indicate that a history of IL stimulation limits net cardiac sympathetic drive during chronic stress in males, an effect that may protect against CVS-increased FS. Conversely, neither CVS nor prior IL stimulation affected autonomic balance or cardiac function in females. However, acute IL stimulation after CVS increased female cardiac contractility.

Chronic stress effects on cardiac structure

Left ventricular morphological analysis was carried out to examine potential structural contributions to altered function. In YFP males (**Fig. 7A**; n = 8), CVS increased wall thickness of the posterior wall in systole (**Fig 7B**; Wilcoxon: Post vs Pre W = 28, $p < 0.05$) and the anterior wall in both systole (Wilcoxon: Post vs Pre W = 36, $p < 0.01$) and diastole (Wilcoxon: Post vs Pre W = 28, $p < 0.05$). Furthermore, increased wall thickness was sufficient to decrease ventricle size in systole (**Fig. 7C**; Wilcoxon: Post vs Pre W = -30, $p < 0.05$). Critically, male rats that had previously received IL stimulation (ChR2, n = 8) were protected from the effects of CVS on cardiac hypertrophy (**Fig 7D-E**; Wilcoxon: Post vs Pre W = -9 to 20, $p > 0.05$). In contrast to males, female rats (**Fig. 7F**) showed minimal effects of CVS on cardiac remodeling as YFP rats (n = 10) had decreased posterior wall thickness in diastole (**Fig. 7G**; Wilcoxon:

Post vs Pre W = -37.0, $p < 0.05$) with no other structural changes (**Fig. 7H**; $p > 0.05$). Additionally, there were no significant changes in cardiac structure in the female ChR2 group (**Fig. 7I-J**; n = 16, Wilcoxon: Post vs Pre W = -45 to 25, $p > 0.05$). Overall, CVS-induced inward hypertrophic remodeling was prevented by prior IL activation in males. In contrast, female rats were generally resistant to the hypertrophic effects of chronic stress.

Discussion

In the current study, optogenetic stimulation of glutamatergic IL pyramidal neurons was combined with behavioral, endocrine, and cardiovascular assessments. Our results show that, in males, IL pyramidal neuron activity was preferred, increased social motivation, and reduced acute physiological stress reactivity. Intriguingly, prior IL activation lowered net cardiac sympathetic drive and protected against subsequent myocardial remodeling after chronic stress. However, IL activity had fundamentally different regulatory effects in females. Stimulation did not have motivational valence or alter social behavior but increased acute physiological stress reactivity and cardiac contractility following chronic stress. Collectively, these findings identify sexual divergence in the cortical integration of affective and physiological systems, suggesting that vmPFC output signaling may differentially impact health outcomes in males and females.

The comorbidity of CVD and MDD shows sexual divergence with females at twice the risk (Goldstein et al., 2019; Möller-Leimkühler, 2007; Naqvi et al., 2005). Given the interactions between stress, mood disorders, and CVD, stress-reactive neural populations are well positioned to regulate affective and cardiovascular outcomes. Crucially, chronic stress exposure in male rats reduces IL pyramidal neuron dendritic arborization and increases local GABAergic signaling, suggesting reduced glutamatergic output (McKlveen et al., 2019, 2016; Radley et al., 2008). Further, long-term reduction of male IL glutamatergic output increases HPA axis activity and impairs vascular function (Myers et al., 2017; Schaeuble et al., 2019). Collectively, IL output neurons represent a target for modulating behavioral and physiological responses to

stress. Thus, we sought to test this hypothesis through real-time *in vivo* assessments of behavior, physiology, and organ function. Altogether, we found that the neurobiology of emotional behaviors, endocrine-autonomic integration, and cardiovascular outcomes differed substantially between sexes.

The RTPP test was used to assess the affective state of experimental animals by measuring preference or aversion for IL neural activity. Here, male rats preferred the chamber paired with either 10 Hz or 20 Hz stimulation, but the valence of female IL activation was neither positive nor negative. Previous work indicates that male mPFC stimulation reduces social avoidance after social defeat (Covington et al., 2010), yet relatively few studies have examined IL function in females. Although social interaction induces less IL immediate early-gene expression in females than males (Mikosz et al., 2015; Stack et al., 2010), the current study is, to our knowledge, the first examination of IL regulation of female social behavior. IL activity did not alter social behavior in females, indicating a significant sexual divergence in the neural regulation of sociability. However, males exhibited frequency-dependent increases in social motivation. These results suggest that stimulation near the intrinsic pyramidal neuron firing rate (4-10 Hz) (Homayoun and Moghaddam, 2007; Ji and Neugebauer, 2012) is required to increase male social motivation.

Activation of IL glutamatergic neurons also reduced male glucose and corticosterone responses to stress. Conversely, female IL glutamatergic stimulation increased glucose mobilization without affecting corticosterone, suggesting a role in sympatho-excitation. Female IL activity also increased tachycardic responses to stress, while male IL stimulation reduced cardiovascular stress responses including HR and

arterial pressures. These experiments indicate that IL activity has opposing effects on endocrine-autonomic integration in males and females whereby male glutamatergic IL neurons cause widespread inhibition of the stress response and female IL neurons facilitate sympathetic responses.

Chronic stress exposure induced ventricular hypertrophy and increased endocardial FS in males, suggesting that increased wall thickness likely accounted for the increase in FS. This effect was prevented by a history of IL stimulation in males, likely arising from a reduction in symaptho-vagal imbalance throughout CVS. In fact, previous IL stimulation limited resting net sympathetic drive, a major risk for CVD (Thayer et al., 2012; Wulsin et al., 2015). Given that rats received no optic stimulation during CVS and that acute optic status did not impact male FS, this effect was likely driven by stimulation-induced IL plasticity. IL stimulation has been shown to induce persistent morphological changes in males including increased excitatory synapses onto pyramidal neurons, suggesting a prolonged state of enhanced excitability (Fuchikami et al., 2015; Moda-Sava et al., 2019). Thus, lower resting net sympathetic tone and/or reduced sympathetic activity during stressors may have prevented the consequences of chronic stress to induce inward hypertrophic remodeling of the myocardium. These effects were not present in females as hypertrophic remodeling was not evident and acute stimulation increased FS. Collectively, these results indicate that prior male IL glutamatergic activity is sufficient to restrain responses to chronic stress while female IL activity increases cardiac contractility independent of structural changes.

The IL does not directly innervate the neurons that govern endocrine and autonomic stress responses. Accordingly, downstream glutamate signaling from IL

synaptic terminals requires intermediary synapses. The exact circuits engaged by IL pyramidal cells to bring about the observed effects remain to be determined. However, anterograde mapping studies indicate that IL projections widely innervate the forebrain and brainstem (Vertes, 2004; Wood et al., 2018). We previously found that, in males, stress-activated IL neurons innervate local inhibitory GABAergic neurons in the posterior hypothalamus (PH) (Myers et al., 2016). Furthermore, blocking GABAergic tone in the PH reduces social behavior and increases HPA axis reactivity suggesting inhibition of the PH may be important for limiting behavioral and physiological stress responses (Myers et al., 2016). Additionally, IL inputs to the amygdala are critical for fear extinction and reducing anxiety-like behavior (Adhikari et al., 2015; Sierra-Mercado et al., 2011). Interestingly, amygdala-projecting IL neurons are both resistant to stress-induced dendritic retraction as well as sensitive to estrogen (Shansky et al., 2010, 2009). Thus, the IL-amygdala circuit could play a key role in sex differences in behavioral regulation. Although the downstream mechanisms of IL cardiovascular regulation are unknown, male IL projections target pre-autonomic cell groups in the brainstem and give rise to multi-synaptic pathways that innervate the adrenal medulla (Dum et al., 2019; Gabbott et al., 2005). Further sex-specific analysis of IL synaptic signaling in forebrain and brainstem nuclei is necessary to determine the basis of divergent behavioral and physiological integration.

While ovarian hormones have far-reaching effects on behavior and physiological systems, we did not control for estrous cycle phase. Instead, we used randomly cycling females. Cycle phase was reported for each treatment, but statistical power was insufficient to examine phase as a factor. It remains to be determined how gonadal

hormones might contribute to the sexually divergent effects observed. Estrogen receptor (ER) α, β, and the g-protein coupled ER are expressed in pyramidal and non-pyramidal PFC neurons in both sexes (Almey et al., 2014; Montague et al., 2008). Further, ER localized to PFC dendritic spines regulates synaptic morphology and ionotropic glutamate receptor ubiquitination/degradation following repeated stress (Hao et al., 2006; Wei et al., 2014; Yuen et al., 2016). These protective effects are dependent on PFC ERα and estradiol-synthesizing aromatase (Wei et al., 2014), indicating a role for extra-ovarian estrogen synthesis. In addition, ER expressed in axons and axonal terminals rapidly alters pre-synaptic transmission in pyramidal cells (Almey et al., 2014). Although studies have described multiple interactions between ER and cortical glutamate signaling (Galvin and Ninan, 2014; Hara et al., 2018), much less is known about PFC progesterone signaling. Progesterone receptors are expressed in frontal cortex (Guerra-Araiza et al., 2003) but progesterone derivatives also signal through $GABA_A$ receptors and regulate GABA subunit expression (Andrade et al., 2012). Moreover, sex differences in IL regulation of behavior and physiology could arise from the actions of androgens. Androgen receptors (AR) are expressed in PFC neurons and glia (Finley and Kritzer, 1999). AR is also enriched in VTA-projecting PFC neurons that influence extracellular dopamine in PFC through downstream VTA glutamate signaling (Aubele and Kritzer, 2012). It is particularly interesting that androgens and estrogens act in opposition to modify PFC dopamine, norepinephrine, and serotonin metabolism during novel environment stress (Handa et al., 1997). Thus, gonadal steroids and locally synthesized modulators affect PFC cellular processes and projection activity, ultimately engaging multiple neurotransmitter systems. Accordingly, the specific cellular and

synaptic processes contributing to sex-dependent stress reactivity and resilience are promising avenues for identifying therapeutic targets.

The current study identified a cortical node integrating mood-related behaviors with cardiovascular outcomes. Moreover, activity in this vmPFC cell population produced sex-specific effects on behavior and physiology. In addition to highlighting the necessity of sex-based investigation, these data point to a neurochemical basis for sex differences in stress-related health determinants. Ultimately, further investigation of brain-body interactions in the face of prolonged stress may provide a better understating of disease risk and resilience factors.

Acknowledgments

This work was supported by NIH grants R00 HL122454 and R01 HL150559 to Brent Myers. Data generated by the University of Cincinnati Mouse Metabolic Phenotyping Core were supported by NIH grant U2C DK059630. AAV5 vectors were provided by the University of North Carolina Vector Core under material transfer agreement with Karl Deisseroth and Stanford University.

References

Adhikari A, Lerner TN, Finkelstein J, Pak S, Jennings JH, Davidson TJ, Ferenczi E, Gunaydin LA, Mirzabekov JJ, Ye L, Kim SY, Lei A, Deisseroth K. 2015. Basomedial amygdala mediates top-down control of anxiety and fear. *Nature* **527**:179–185. doi:10.1038/nature15698

Almey A, Cannell E, Bertram K, Filardo E, Milner TA, Brake WG. 2014. Medial prefrontal cortical estradiol rapidly alters memory system bias in female rats: Ultrastructural analysis reveals membrane-associated estrogen receptors as potential mediators. *Endocrinology* **155**:4422–4432. doi:10.1210/en.2014-1463

Andrade S, Arbo BD, Batista BAM, Neves AM, Branchini G, Brum IS, Barros HMT, Gomez R, Ribeiro MFM. 2012. Effect of progesterone on the expression of GABA $_A$ receptor subunits in the prefrontal cortex of rats: implications of sex differences and brain hemisphere. *Cell Biochem Funct* **30**:696–700. doi:10.1002/cbf.2854

Aubele T, Kritzer MF. 2012. Androgen influence on prefrontal dopamine systems in adult male rats: Localization of cognate intracellular receptors in medial prefrontal projections to the ventral tegmental area and effects of gonadectomy and hormone replacement on glutamate-stimulated extracellular dopamine level. *Cereb Cortex* **22**:1799–1812. doi:10.1093/cercor/bhr258

Beckmann M, Johansen-Berg H, Rushworth MFS. 2009. Connectivity-based parcellation of human cingulate cortex and its relation to functional specialization. *J Neurosci* **29**:1175–1190. doi:10.1523/JNEUROSCI.3328-08.2009

Beissner F, Meissner K, Bär KJ, Napadow V. 2013. The autonomic brain: An activation likelihood estimation meta-analysis for central processing of autonomic function. *J Neurosci* **33**:10503–10511. doi:10.1523/JNEUROSCI.1103-13.2013

Bimpisidis Z, König N, Wallén-Mackenzie Å. 2020. Two different real-time place preference paradigms using optogenetics within the ventral tegmental area of the mouse. *J Vis Exp* **2020**:60867. doi:10.3791/60867

Binder EB, Nemeroff CB. 2010. The CRF system, stress, depression and anxietyinsights from human genetic studies. *Mol Psychiatry*. doi:10.1038/mp.2009.141

Caballero JP, Scarpa GB, Remage-Healey L, Moorman DE. 2019. Differential Effects of Dorsal and Ventral Medial Prefrontal Cortex Inactivation during Natural Reward Seeking, Extinction, and Cue-Induced Reinstatement. *eneuro* **6**:ENEURO.0296-19.2019. doi:10.1523/eneuro.0296-19.2019

Chicco AJ, McCune SA, Emter CA, Sparagna GC, Rees ML, Bolden DA, Marshall KD, Murphy RC, Moore RL. 2008. Low-intensity exercise training delays heart failure and improves survival in female hypertensive heart failure rats. *Hypertension* **51**:1096–1102. doi:10.1161/HYPERTENSIONAHA.107.107078

Cora MC, Kooistra L, Travlos G. 2015. Vaginal Cytology of the Laboratory Rat and Mouse:Review and Criteria for the Staging of the Estrous Cycle Using Stained Vaginal Smears. *Toxicol Pathol* **43**:776–793. doi:10.1177/0192623315570339

Covington HE, Lobo MK, Maze I, Vialou V, Hyman JM, Zaman S, LaPlant Q, Mouzon E, Ghose S, Tamminga CA, Neve RL, Deisseroth K, Nestler EJ. 2010. Antidepressant effect of optogenetic stimulation of the medial prefrontal cortex. *J Neurosci* **30**:16082–16090. doi:10.1523/JNEUROSCI.1731-10.2010

Dum RP, Levinthal DJ, Strick PL. 2019. The mind-body problem: Circuits that link the cerebral cortex to the adrenal medulla. *Proc Natl Acad Sci U S A* **116**:26321–26328. doi:10.1073/pnas.1902297116

Electrophysiology TF of the ES. 1996. Heart Rate Variability. *Circulation* **93**:1043–1065. doi:10.1161/01.CIR.93.5.1043

Felix-Ortiz AC, Tye KM. 2014. Amygdala inputs to the ventral hippocampus bidirectionally modulate social behavior. *J Neurosci* **34**:586–595. doi:10.1523/JNEUROSCI.4257-13.2014

Finley SK, Kritzer MF. 1999. Immunoreactivity for intracellular androgen receptors in identified subpopulations of neurons, astrocytes and oligodendrocytes in primate prefrontal cortex. *J Neurobiol* **40**:446–457. doi:10.1002/(SICI)1097-4695(19990915)40:4<446::AID-NEU3>3.0.CO;2-J

Flak JN, Jankord R, Solomon MB, Krause EG, Herman JP. 2011. Opposing effects of chronic stress and weight restriction on cardiovascular, neuroendocrine and metabolic function. *Physiol Behav* **104**:228–234. doi:10.1016/j.physbeh.2011.03.002

Fuchikami M, Thomas A, Liu R, Wohleb ES, Land BB, DiLeone RJ, Aghajanian GK, Duman RS. 2015. Optogenetic stimulation of infralimbic PFC reproduces ketamine's rapid and sustained antidepressant actions. *Proc Natl Acad Sci U S A* **112**:8106–8111. doi:10.1073/pnas.1414728112

Gabbott PLA, Warner TA, Jays PRL, Salway P, Busby SJ. 2005. Prefrontal cortex in the rat: Projections to subcortical autonomic, motor, and limbic centers. *J Comp Neurol* **492**:145–177. doi:10.1002/cne.20738

Galvin C, Ninan I. 2014. Regulation of the mouse medial prefrontal cortical synapses by endogenous estradiol. *Neuropsychopharmacology* **39**:2086–2094. doi:10.1038/npp.2014.56

Gianaros PJ, Sheu LK. 2009. A review of neuroimaging studies of stressor-evoked blood pressure reactivity: Emerging evidence for a brain-body pathway to coronary heart disease risk. *Neuroimage*. doi:10.1016/j.neuroimage.2009.04.073

Gianaros PJ, Wager TD. 2015. Brain-Body Pathways Linking Psychological Stress and Physical Health. *Curr Dir Psychol Sci* **24**:313–321. doi:10.1177/0963721415581476

Goldstein JM, Hale T, Foster SL, Tobet SA, Handa RJ. 2019. Sex differences in major depression and comorbidity of cardiometabolic disorders: impact of prenatal stress and immune exposures. *Neuropsychopharmacology*. doi:10.1038/s41386-018-0146-1

Goodson ML, Packard AEB, Buesing DR, Maney M, Myers B, Fang Y, Basford JE, Hui DY, Ulrich-Lai YM, Herman JP, Ryan KK. 2017. Chronic stress and Rosiglitazone increase indices of vascular stiffness in male rats. *Physiol Behav* **172**:16–23. doi:10.1016/j.physbeh.2016.03.031

Grippo AJ, Johnson AK. 2009. Stress, depression and cardiovascular dysregulation: A review of neurobiological mechanisms and the integration of research from preclinical disease models. *Stress*. doi:10.1080/10253890802046281

Guerra-Araiza C, Villamar-Cruz O, González-Arenas A, Chavira R, Camacho-Arroyo I. 2003. Changes in progestrone receptor isoforms content in the rat brain during the oestrous cycle and after oestradiol and progesterone treatments. *J Neuroendocrinol* **15**:984–990. doi:10.1046/j.1365-2826.2003.01088.x

Handa RJ, Hejna GM, Lorens SA. 1997. Androgen inhibits neurotransmitter turnover in the medial prefrontal cortex of the rat following exposure to a novel environment. *Brain Res* **751**:131–138. doi:10.1016/S0006-8993(96)01394-7

Hao J, Rapp PR, Leffler AE, Leffler SR, Janssen WGM, Lou W, McKay H, Roberts JA, Wearne SL, Hof PR, Morrison JH. 2006. Estrogen alters spine number and morphology in prefrontal cortex of aged female rhesus monkeys. *J Neurosci* **26**:2571–2578. doi:10.1523/JNEUROSCI.3440-05.2006

Hara Y, Crimins JL, Puri R, Wang ACJ, Motley SE, Yuk F, Ramos TM, Janssen WGM, Rapp PR, Morrison JH. 2018. Estrogen Alters the Synaptic Distribution of Phospho-GluN2B in the Dorsolateral Prefrontal Cortex While Promoting Working Memory in Aged Rhesus Monkeys. *Neuroscience* **394**:303–315. doi:10.1016/j.neuroscience.2018.09.021

Homayoun H, Moghaddam B. 2007. NMDA receptor hypofunction produces opposite effects on prefrontal cortex interneurons and pyramidal neurons. *J Neurosci* **27**:11496–11500. doi:10.1523/JNEUROSCI.2213-07.2007

Ji G, Neugebauer V. 2012. Modulation of medial prefrontal cortical activity using in vivo recordings and optogenetics. *Mol Brain* **5**:36. doi:10.1186/1756-6606-5-36

Le CH, Mulligan CM, Routh MA, Bouma GJ, Frye MA, Jeckel KM, Sparagna GC, Lynch JM, Moore RL, McCune SA, Bristow M, Zarini S, Murphy RC, Chicco AJ. 2014. Delta-6-desaturase links polyunsaturated fatty acid metabolism with phospholipid remodeling and disease progression in heart failure. *Circ Hear Fail* **7**:172–183. doi:10.1161/CIRCHEARTFAILURE.113.000744

Liotti M, Mayberg HS, Brannan SK, McGinnis S, Jerabek P, Fox PT. 2000. Differential limbic-cortical correlates of sadness and anxiety in healthy subjects: Implications for affective disorders. *Biol Psychiatry* **48**:30–42. doi:10.1016/S0006-3223(00)00874-X

Mayberg HS, Lozano AM, Voon V, McNeely HE, Seminowicz D, Hamani C, Schwalb JM, Kennedy SH. 2005. Deep brain stimulation for treatment-resistant depression. *Neuron* **45**:651–660. doi:10.1016/j.neuron.2005.02.014

McKlveen JM, Moloney RD, Scheimann JR, Myers B, Herman JP. 2019. “Braking” the Prefrontal Cortex: The Role of Glucocorticoids and Interneurons in Stress Adaptation and Pathology. *Biol Psychiatry*. doi:10.1016/j.biopsych.2019.04.032

McKlveen JM, Morano RL, Fitzgerald M, Zoubovsky S, Cassella SN, Scheimann JR, Ghosal S, Mahbod P, Packard BA, Myers B, Baccei ML, Herman JP. 2016. Chronic Stress Increases Prefrontal Inhibition: A Mechanism for Stress-Induced Prefrontal Dysfunction. *Biol Psychiatry* **80**:754–764. doi:10.1016/j.biopsych.2016.03.2101

McKlveen JM, Myers B, Herman JP. 2015. The Medial Prefrontal Cortex: Coordinator of Autonomic, Neuroendocrine and Behavioural Responses to Stress. *J Neuroendocrinol*. doi:10.1111/jne.12272

Mikosz M, Nowak A, Werka T, Knapska E. 2015. Sex differences in social modulation of learning in rats. *Sci Rep* **5**. doi:10.1038/srep18114

Moda-Sava RN, Murdock MH, Parekh PK, Fetcho RN, Huang BS, Huynh TN, Witztum J, Shaver DC, Rosenthal DL, Alway EJ, Lopez K, Meng Y, Nellissen L, Grosenick L, Milner TA, Deisseroth K, Bito H, Kasai H, Liston C. 2019. Sustained rescue of prefrontal circuit dysfunction by antidepressant-induced spine formation. *Science (80-)* **364**. doi:10.1126/science.aat8078

Möller-Leimkühler AM. 2007. Gender differences in cardiovascular disease and comorbid depression. *Dialogues Clin Neurosci* **9**:71–83.
Montague D, Weickert CS, Tomaskovic-Crook E, Rothmond DA, Kleinman JE, Rubinow DR. 2008. Oestrogen receptor α localisation in the prefrontal cortex of three mammalian species. *J Neuroendocrinol* **20**:893–903. doi:10.1111/j.1365-2826.2008.01743.x
Moy SS, Nadler JJ, Perez A, Barbaro RP, Johns JM, Magnuson TR, Piven J, Crawley JN. 2004. Sociability and preference for social novelty in five inbred strains: An approach to assess autistic-like behavior in mice. *Genes, Brain Behav* **3**:287–302. doi:10.1111/j.1601-1848.2004.00076.x
Myers-Schulz B, Koenigs M. 2012. Functional anatomy of ventromedial prefrontal cortex: Implications for mood and anxiety disorders. *Mol Psychiatry*. doi:10.1038/mp.2011.88
Myers B. 2016. Corticolimbic regulation of cardiovascular responses to stress. *Physiol Behav* **172**:49–59. doi:10.1016/j.physbeh.2016.10.015
Myers B, Carvalho-Netto E, Wick-Carlson D, Wu C, Naser S, Solomon MB, Ulrich-Lai YM, Herman JP. 2016. GABAergic Signaling within a Limbic-Hypothalamic Circuit Integrates Social and Anxiety-Like Behavior with Stress Reactivity. *Neuropsychopharmacology* **41**:1530–9. doi:10.1038/npp.2015.311
Myers B, Mark Dolgas C, Kasckow J, Cullinan WE, Herman JP. 2014a. Central stress-integrative circuits: Forebrain glutamatergic and GABAergic projections to the dorsomedial hypothalamus, medial preoptic area, and bed nucleus of the stria terminalis. *Brain Struct Funct* **219**. doi:10.1007/s00429-013-0566-y
Myers B, McKlveen JM, Herman JP. 2014b. Glucocorticoid actions on synapses, circuits, and behavior: Implications for the energetics of stress. *Front Neuroendocrinol*. doi:10.1016/j.yfrne.2013.12.003
Myers B, McKlveen JM, Morano R, Ulrich-Lai YM, Solomon MB, Wilson SP, Herman JP. 2017. Vesicular Glutamate Transporter 1 Knockdown in Infralimbic Prefrontal Cortex Augments Neuroendocrine Responses to Chronic Stress in Male Rats. *Endocrinology* **158**:3579–3591. doi:10.1210/en.2017-00426
Naqvi TZ, Naqvi SSA, Merz CNB. 2005. Gender differences in the link between depression and cardiovascular disease. *Psychosom Med*. doi:10.1097/01.psy.0000164013.55453.05
Öngür D, Ferry AT, Price JL. 2003. Architectonic subdivision of the human orbital and medial prefrontal cortex. *J Comp Neurol* **460**:425–449. doi:10.1002/cne.10609
Radley JJ, Rocher AB, Rodriguez A, Ehlenberger DB, Dammann M, Mcewen BS, Morrison JH, Wearne SL, Hof PR. 2008. Repeated stress alters dendritic spine morphology in the rat medial prefrontal cortex. *J Comp Neurol* **507**:1141–1150. doi:10.1002/cne.21588
Rau AR, Hentges ST. 2017. The relevance of AgRP neuron-derived GABA inputs to POMC neurons differs for spontaneous and evoked release. *J Neurosci* **37**:7362–7372. doi:10.1523/JNEUROSCI.0647-17.2017
Sankar T, Chakravarty MM, Jawa N, Li SX, Giacobbe P, Kennedy SH, Rizvi SJ, Mayberg HS, Hamani C, Lozano AM. 2019. Neuroanatomical predictors of response to subcallosal cingulate deep brain stimulation for treatment-resistant depression. *J Psychiatry Neurosci* **44**:1–10. doi:10.1503/jpn.180207

Schaeuble D, Packard AEB, McKlveen JM, Morano R, Fourman S, Smith BL, Scheimann JR, Packard BA, Wilson SP, James J, Hui DY, Ulrich-Lai YM, Herman JP, Myers B. 2019. Prefrontal Cortex Regulates Chronic Stress-Induced Cardiovascular Susceptibility. *J Am Heart Assoc* **8**:e014451. doi:10.1161/JAHA.119.014451

Selimbeyoglu A, Kim CK, Inoue M, Lee SY, Hong ASO, Kauvar I, Ramakrishnan C, Fenno LE, Davidson TJ, Wright M, Deisseroth K. 2017. Modulation of prefrontal cortex excitation/inhibition balance rescues social behavior in CNTNAP2-deficient mice. *Sci Transl Med* **9**:eaah6733. doi:10.1126/scitranslmed.aah6733

Sgoifo A, Carnevali L, Pico Alfonso MDLA, Amore M. 2015. Autonomic dysfunction and heart rate variability in depression. *Stress*. doi:10.3109/10253890.2015.1045868

Shansky RM, Hamo C, Hof PR, Lou W, McEwen BS, Morrison JH. 2010. Estrogen promotes stress sensitivity in a prefrontal cortex-amygdala pathway. *Cereb Cortex* **20**:2560–2567. doi:10.1093/cercor/bhq003

Shansky RM, Hamo C, Hof PR, McEwen BS, Morrison JH. 2009. Stress-induced dendritic remodeling in the prefrontal cortex is circuit specific. *Cereb Cortex* **19**:2479–2484. doi:10.1093/cercor/bhp003

Shoemaker JK, Badrov MB, Al-Khazraji BK, Jackson DN. 2016. Neural control of vascular function in skeletal muscle. *Compr Physiol* **6**:303–329. doi:10.1002/cphy.c150004

Sierra-Mercado D, Padilla-Coreano N, Quirk GJ. 2011. Dissociable roles of prelimbic and infralimbic cortices, ventral hippocampus, and basolateral amygdala in the expression and extinction of conditioned fear. *Neuropsychopharmacology* **36**:529–538. doi:10.1038/npp.2010.184

Smith BL, Morano RL, Ulrich-Lai YM, Myers B, Solomon MB, Herman JP. Adolescent environmental enrichment prevents behavioral and physiological sequelae of adolescent chronic stress in female (but not male) rats. *Stress* **21**. doi:10.1080/10253890.2017.1402883

Solomon MB, Loftspring M, De Kloet AD, Ghosal S, Jankord R, Flak JN, Wulsin AC, Krause EG, Zhang R, Rice T, McKlveen J, Myers B, Tasker JG, Herman JP. 2015. Neuroendocrine function after hypothalamic depletion of glucocorticoid receptors in male and female mice. *Endocrinology* **156**:2843–2853. doi:10.1210/en.2015-1276

Stack A, Carrier N, Dietz D, Hollis F, Sorenson J, Kabbaj M. 2010. Sex differences in social interaction in rats: Role of the immediate-early gene zif268. *Neuropsychopharmacology* **35**:570–580. doi:10.1038/npp.2009.163

Stamatakis AM, Stuber GD. 2012. Activation of lateral habenula inputs to the ventral midbrain promotes behavioral avoidance. *Nat Neurosci* **15**:1105–1107. doi:10.1038/nn.3145

Thayer JF, Åhs F, Fredrikson M, Sollers JJ, Wager TD. 2012. A meta-analysis of heart rate variability and neuroimaging studies: Implications for heart rate variability as a marker of stress and health. *Neurosci Biobehav Rev*. doi:10.1016/j.neubiorev.2011.11.009

Uylings HBM, Groenewegen HJ, Kolb B. 2003. Do rats have a prefrontal cortex? *Behav Brain Res*. doi:10.1016/j.bbr.2003.09.028

Vahl TP, Ulrich-Lai YM, Ostrander MM, Dolgas CM, Elfers EE, Seeley RJ, D'Alessio DA, Herman JP. 2005. Comparative analysis of ACTH and corticosterone sampling

methods in rats. *Am J Physiol Endocrinol Metab* **289**:E823-8. doi:10.1152/ajpendo.00122.2005
van Holstein M, Floresco SB. 2019. Dissociable roles for the ventral and dorsal medial prefrontal cortex in cue-guided risk/reward decision making. *Neuropsychopharmacology*. doi:10.1038/s41386-019-0557-7
Vertes RP. 2004. Differential Projections of the Infralimbic and Prelimbic Cortex in the Rat. *Synapse* **51**:32–58. doi:10.1002/syn.10279
Vijayakumar N, Cheng TW, Pfeifer JH. 2017. Neural correlates of social exclusion across ages: A coordinate-based meta-analysis of functional MRI studies. *Neuroimage*. doi:10.1016/j.neuroimage.2017.02.050
Wei J, Yuen EY, Liu W, Li X, Zhong P, Karatsoreos IN, McEwen BS, Yan Z. 2014. Estrogen protects against the detrimental effects of repeated stress on glutamatergic transmission and cognition. *Mol Psychiatry* **19**:588–598. doi:10.1038/mp.2013.83
Wood JN, Grafman J. 2003. Human prefrontal cortex: Processing and representational perspectives. *Nat Rev Neurosci* **4**:139–147. doi:10.1038/nrn1033
Wood M, Adil O, Wallace T, Fourman S, Wilson SP, Herman JP, Myers B. 2018. Infralimbic prefrontal cortex structural and functional connectivity with the limbic forebrain: a combined viral genetic and optogenetic analysis. *Brain Struct Funct* 1–25. doi:10.1007/s00429-018-1762-6
Wulsin LR, Horn PS, Perry JL, Massaro JM, D'Agostino RB. 2015. Autonomic Imbalance as a Predictor of Metabolic Risks, Cardiovascular Disease, Diabetes, and Mortality. *J Clin Endocrinol Metab* **100**:2443–2448. doi:10.1210/jc.2015-1748
Yuen EY, Wei J, Yan Z. 2016. Estrogen in prefrontal cortex blocks stress-induced cognitive impairments in female rats. *J Steroid Biochem Mol Biol*. doi:10.1016/j.jsbmb.2015.08.028

Figure Legends

Figure 1: Approach validation and experimental design. (**A**) Injection of AAV-packaged constructs led to expression of cytosolic YFP or membrane-targeted ChR2-YFP under the CaMKIIα promoter. Blue light stimulation in ChR2 females (5 min, 1 mW, 10 Hz, 5 ms pulse) led to robust expression of the immediate-early gene marker c-Fos. White arrows indicate representative c-Fos-positive nuclei. Scale bar: 200 µm and 40 µm for combined. (**B**) Voltage-clamp recordings from male IL-containing slices illustrated light-evoked depolarizing current. (**C**) Current-clamp recordings found stimulation-locked spiking with 10 and 20 Hz stimulation. (**D**) Experimental timelines. RTPP: real-time place preference, SI: social interaction, RS: restraint stress, NE: novel environment, CVS: chronic variable stress. (**E**) Optic fiber placements (YFP: yellow, ChR2: blue) were mapped within or immediately dorsal to the IL (red outline). Coronal sections adapted from Swanson Rat Brain Atlas (3rd edition).

Figure 2: IL pyramidal neuron activity was preferred in males but not females. (**A**) Heat maps illustrate mean animal position in RTPP arena on stimulation day (n = 10 - 15/group). (**B**) Male ChR2 rats preferred the chamber paired with 20 Hz or 10 Hz stimulation relative to habituation day and YFP controls. Females showed no preference or aversion for IL stimulation. ** $p < 0.01$, *** $p < 0.001$ vs. YFP within stimulation. $^{\#\#}$ $p < 0.01$ vs. habituation within ChR2. Inset: portion of rats in each estrous cycle phase. D: diestrus, P: proestrus, M: metestrus, E: estrous. (**C**) Total distance traveled during stimulation found no treatment-based differences in locomotion.

Figure 3: IL stimulation increased social motivation in males but not females. (**A**) Representative movement traces during the social interaction test (n = 7-16/group). (**B**) Interaction, defined as nose-poke onto social cage, was increased by 10 Hz stimulation in males but not 20 Hz in males or 10 Hz in females. ** $p < 0.01$ vs. YFP. Inset: portion of rats in each estrous cycle phase. D: diestrus, P: proestrus, M: metestrus, E: estrous.

Figure 4: IL activation during acute restraint stress attenuated endocrine responses in males but increased female stress reactivity. Stimulation (blue shading) during restraint lowered plasma corticosterone **(A)** and blood glucose **(B)** in ChR2 males. **(C)** Stimulation in females did not alter corticosterone responses. Inset: portion of rats in each estrous cycle phase. D: diestrus, P: proestrus, M: metestrus, E: estrous. **(D)** IL stimulation during restraint increased glucose mobilization in ChR2 females. n = 10-17/group, * $p < 0.05$, ** $p < 0.01$ vs. YFP.

Figure 5: Activation of glutamatergic IL neurons during novel environment exposure reduced male cardiovascular stress responses but increased female HR reactivity. (A) Male IL activation did not affect mean activity in the novel environment. Despite an increase in MAP and DAP during the first minute of stimulation and stress, all recorded hemodynamic responses were decreased in ChR2 males **(B-E)**. **(F)** Stimulation did not alter activity in females. **(G)** Female IL stimulation elevated HR reactivity compared to YFP controls but did not affect arterial pressures **(H-J)**. Inset:

portion of rats in each estrous cycle phase. D: diestrus, P: proestrus, M: metestrus, E: estrous. n = 7-8/group, * $p < 0.05$ vs. YFP.

Figure 6: The effects of chronic stress and IL activity on cardiac function. (A) The ratio of LF to HF components of HRV were reduced in ChR2 males at baseline and the end of CVS. **(B)** Females had no treatment-based effects on net sympathetic drive. L: light phase, D: dark phase, LF: low frequency, HF: high frequency, HRV: heart rate variability. **(C)** CVS increased FS in YFP but not ChR2 males. **(D)** Acute optic status (On vs. Off) did not affect FS in males. **(E)** Females showed no changes in FS after CVS. **(F)** However, acute optogenetic activation increased female FS after CVS. * $p < 0.05$ vs YFP or Pre CVS YFP, ** $p < 0.01$ vs. ChR2 Off.

Figure 7: Effects of chronic stress and prior IL stimulation on cardiac structure. (A) Representative echocardiographic images of the left ventricle in bisected m-mode view before and after CVS in YFP males. V: ventricle, A: anterior wall, P: posterior wall. **(B)** CVS increased wall thickness in diastole and systole in YFP males, **(C)** reducing ventricle size. **(D, E)** ChR2 males that received prior stimulation were protected from the cardiac consequences of CVS. **(F)** Representative m-mode view of the left ventricle in YFP females before and after CVS. **(G, H)** Females did not exhibit ventricular hypertrophy after CVS as posterior wall thickness in diastole was decreased. **(I, J)** No myocardial structural changes were evident in ChR2 females. n = 8-16/group, * $p < 0.05$, ** $p < 0.01$ vs. Pre CVS YFP.

Table 1: Social novelty preference.
Time spent interacting with novel and familiar rats. Stimulation of IL pyramidal neurons did not affect preference for social novelty in males or females.

Experiment	Virus	Novel interaction (% time)	Novel interaction (SEM)	Familiar interaction (% time)	Familiar interaction (SEM)	n
Male 20 Hz	YFP	16.63	1.27	13.06	2.81	7
	ChR2	12.84	1.72	9.73	0.94	10
Male 10 Hz	YFP	16.43	2.07	13.13	2.17	12
	ChR2	18.19	1.81	16.32	2.47	10
Female 10 Hz	YFP	24.84	2.61	16.56	1.62	12
	ChR2	21.58	1.55	16.96	1.51	16

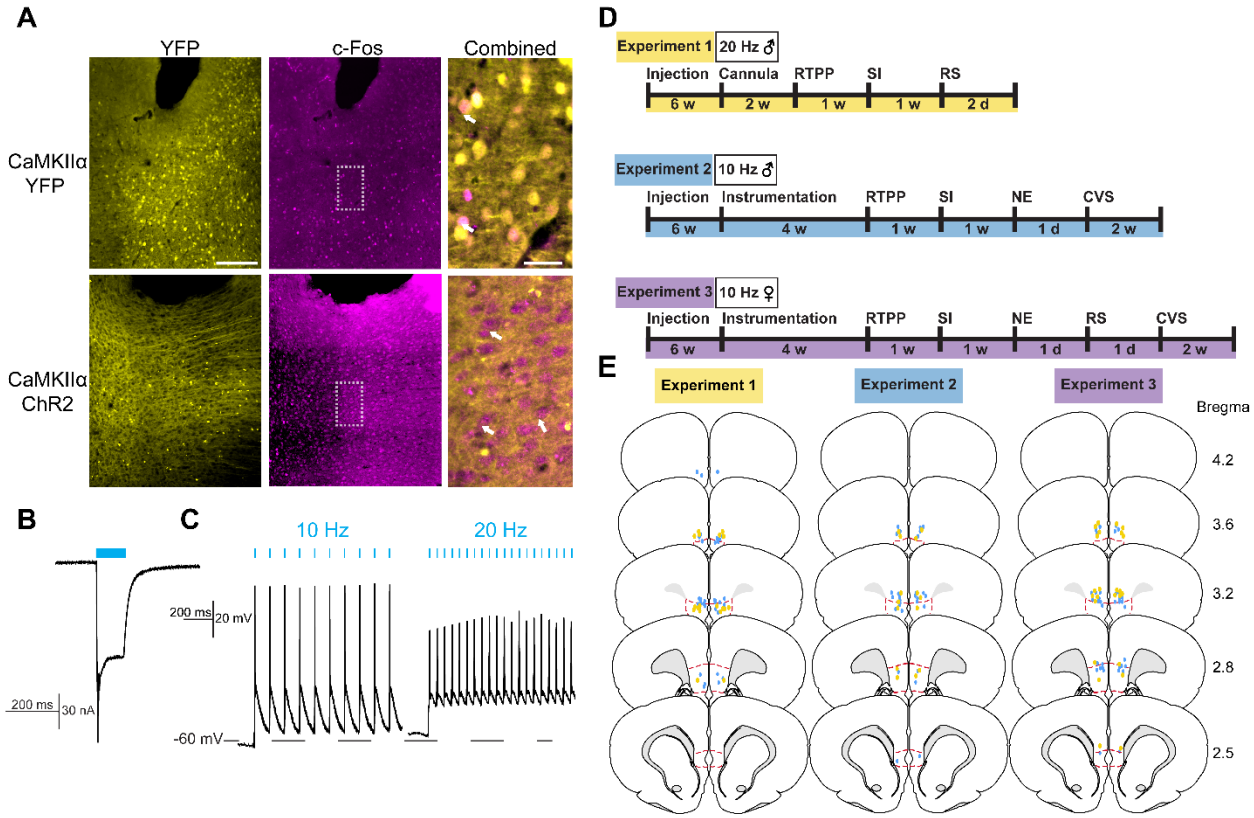

Figure 1: Approach validation and experimental design. (**A**) Injection of AAV-packaged constructs led to expression of cytosolic YFP or membrane-targeted ChR2-YFP under the CaMKIIα promoter. Blue light stimulation in ChR2 females (5 min, 1 mW, 10 Hz, 5 ms pulse) led to robust expression of the immediate-early gene marker c-Fos. White arrows indicate representative c-Fos-positive nuclei. Scale bar: 200 µm and 40 µm for combined. (**B**) Voltage-clamp recordings from male IL-containing slices illustrated light-evoked depolarizing current. (**C**) Current-clamp recordings found stimulation-locked spiking with 10 and 20 Hz stimulation. (**D**) Experimental timelines. RTPP: real-time place preference, SI: social interaction, RS: restraint stress, NE: novel environment, CVS: chronic variable stress. (**E**) Optic fiber placements (YFP: yellow, ChR2: blue) were mapped within or immediately dorsal to the IL (red outline). Coronal sections adapted from Swanson Rat Brain Atlas (3rd edition).

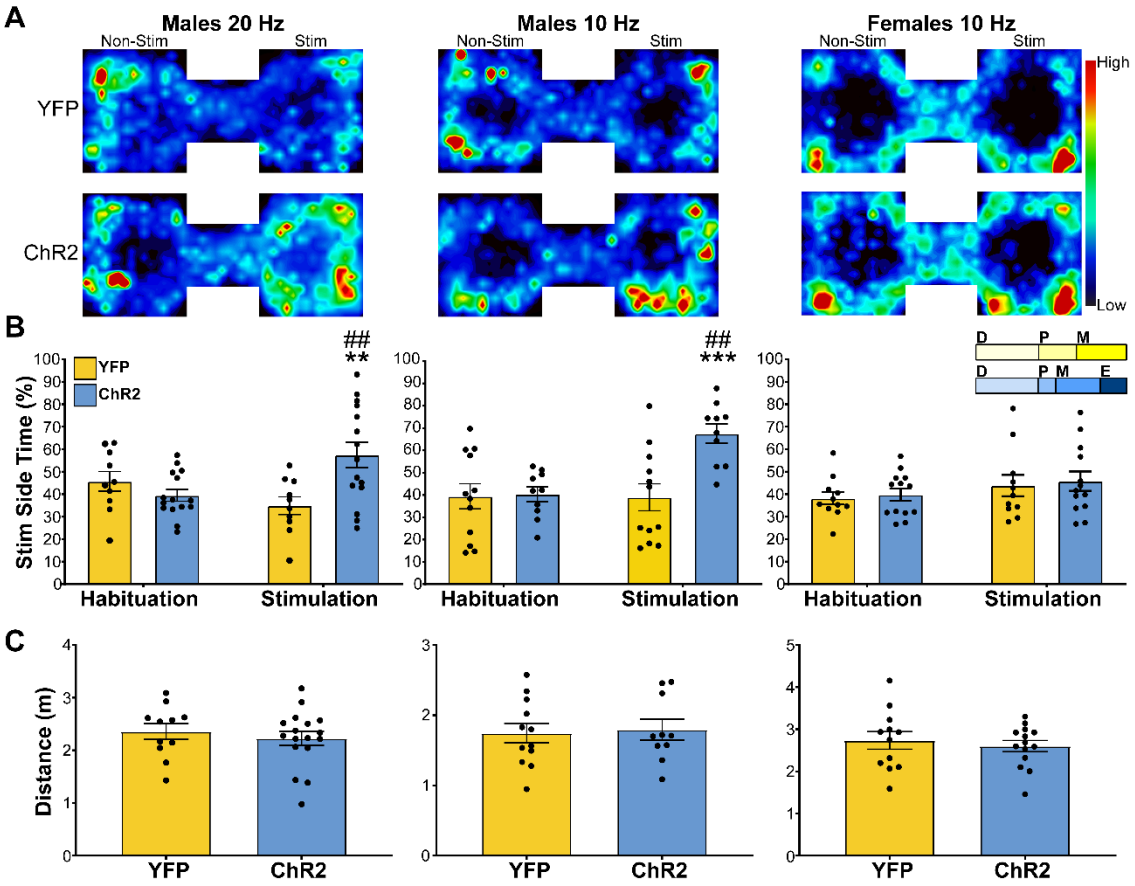

Figure 2: IL pyramidal neuron activity was preferred in males but not females. (**A**) Heat maps illustrate mean animal position in RTPP arena on stimulation day (n = 10 - 15/group). (**B**) Male ChR2 rats preferred the chamber paired with 20 Hz or 10 Hz stimulation relative to habituation day and YFP controls. Females showed no preference or aversion for IL stimulation. ** $p < 0.01$, *** $p < 0.001$ vs. YFP within stimulation. ## $p < 0.01$ vs. habituation within ChR2. Inset: portion of rats in each estrous cycle phase. D: diestrus, P: proestrus, M: metestrus, E: estrous. (**C**) Total distance traveled during stimulation found no treatment-based differences in locomotion.

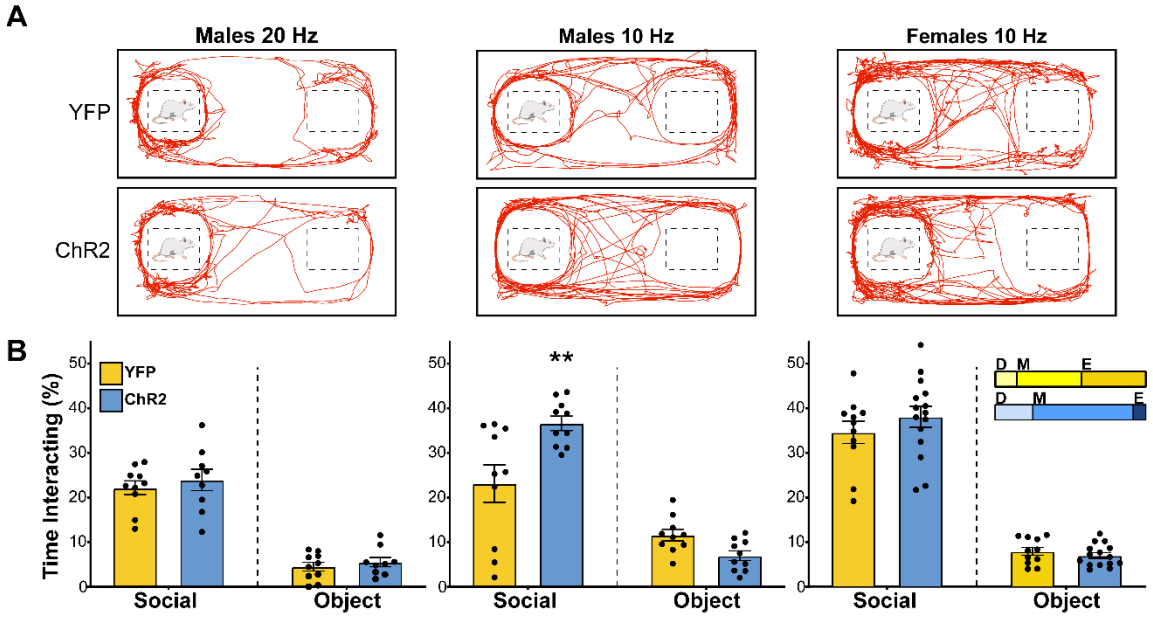

Figure 3: IL stimulation increased social motivation in males but not females. (**A**) Representative movement traces during the social interaction test (n = 7-16/group). (**B**) Interaction, defined as nose-poke onto social cage, was increased by 10 Hz stimulation in males but not 20 Hz in males or 10 Hz in females. ** $p < 0.01$ vs. YFP. Inset: portion of rats in each estrous cycle phase. D: diestrus, P: proestrus, M: metestrus, E: estrous.

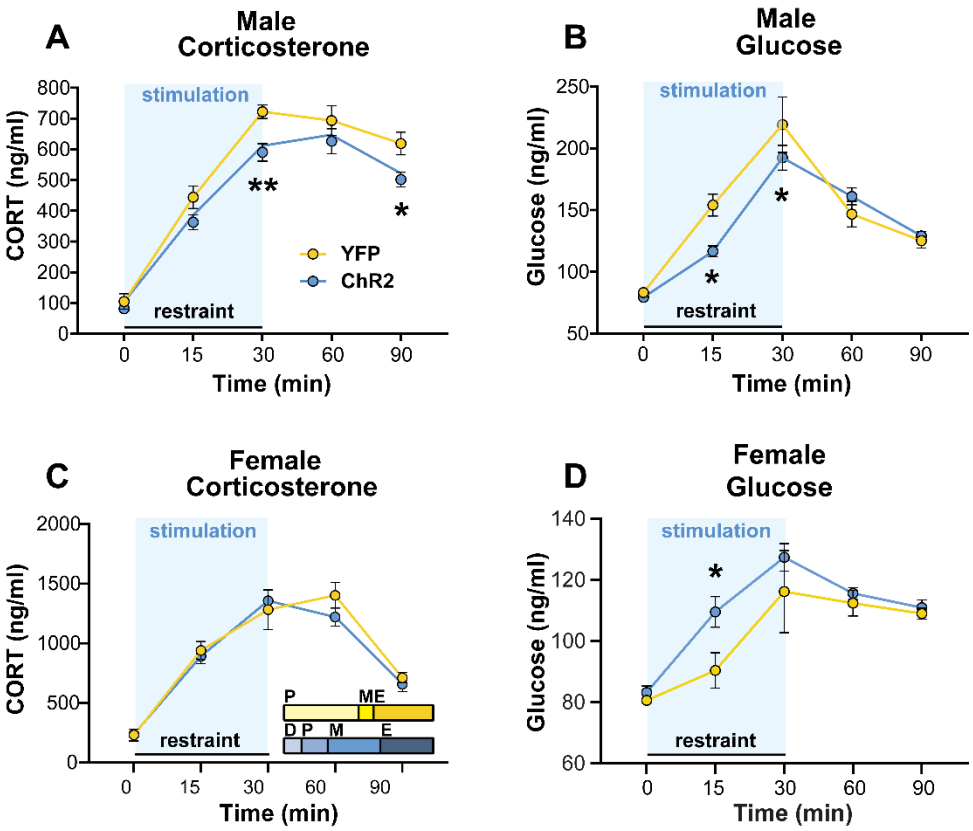

Figure 4: IL activation during acute restraint stress attenuated endocrine responses in males but increased female stress reactivity. Stimulation (blue shading) during restraint lowered plasma corticosterone **(A)** and blood glucose **(B)** in ChR2 males. **(C)** Stimulation in females did not alter corticosterone responses. Inset: portion of rats in each estrous cycle phase. D: diestrus, P: proestrus, M: metestrus, E: estrous. **(D)** IL stimulation during restraint increased glucose mobilization in ChR2 females. n = 10-17/group, * $p < 0.05$, ** $p < 0.01$ vs. YFP.

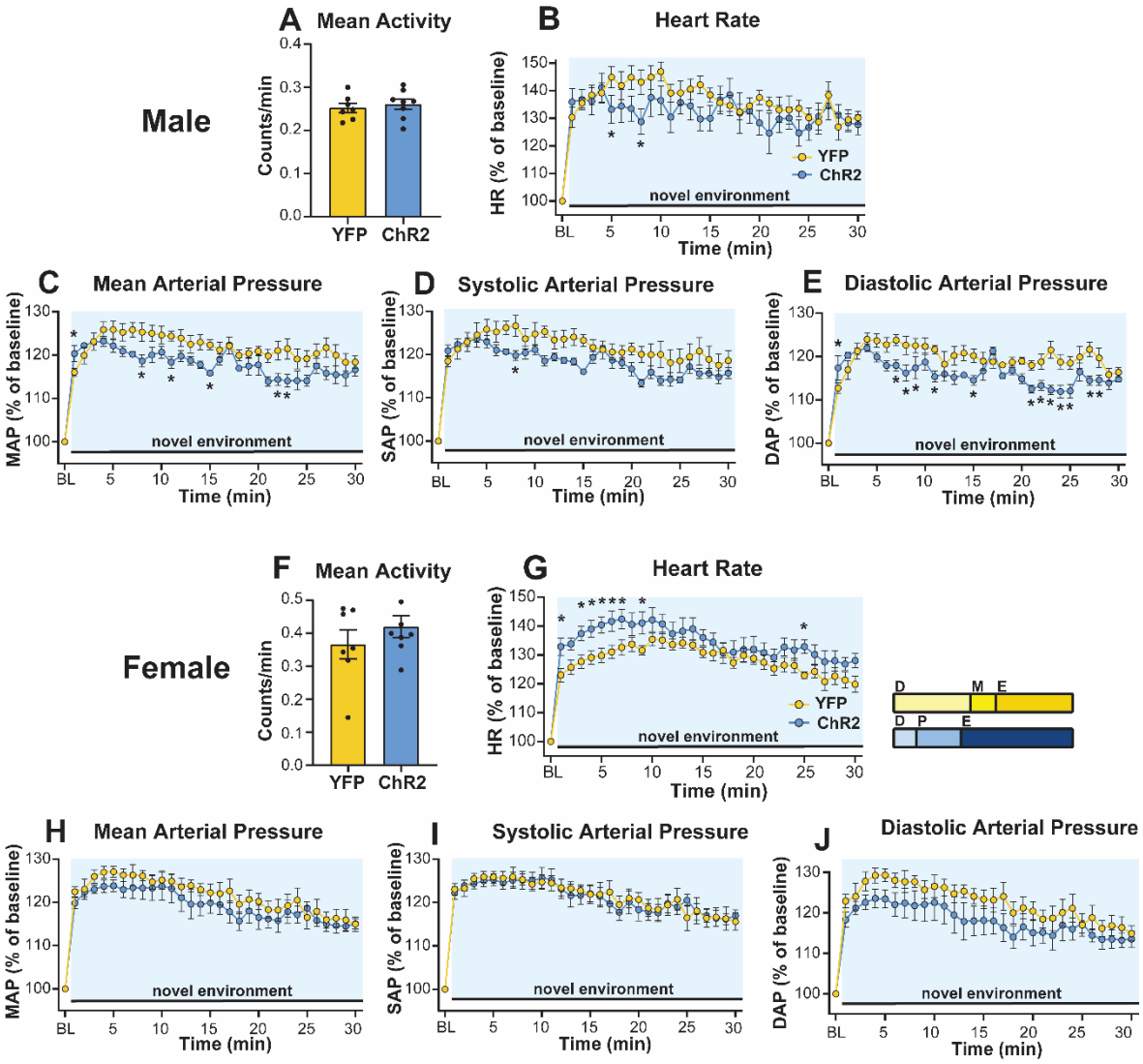

Figure 5: Activation of glutamatergic IL neurons during novel environment exposure reduced male cardiovascular stress responses but increased female HR reactivity. (A) Male IL activation did not affect mean activity in the novel environment. Despite an increase in MAP and DAP during the first minute of stimulation and stress, all recorded hemodynamic responses were decreased in ChR2 males **(B-E)**. **(F)** Stimulation did not alter activity in females. **(G)** Female IL stimulation elevated HR reactivity compared to YFP controls but did not affect arterial pressures **(H-J)**. Inset: portion of rats in each estrous cycle phase. D: diestrus, P: proestrus, M: metestrus, E: estrous. n = 7-8/group, * $p < 0.05$ vs. YFP.

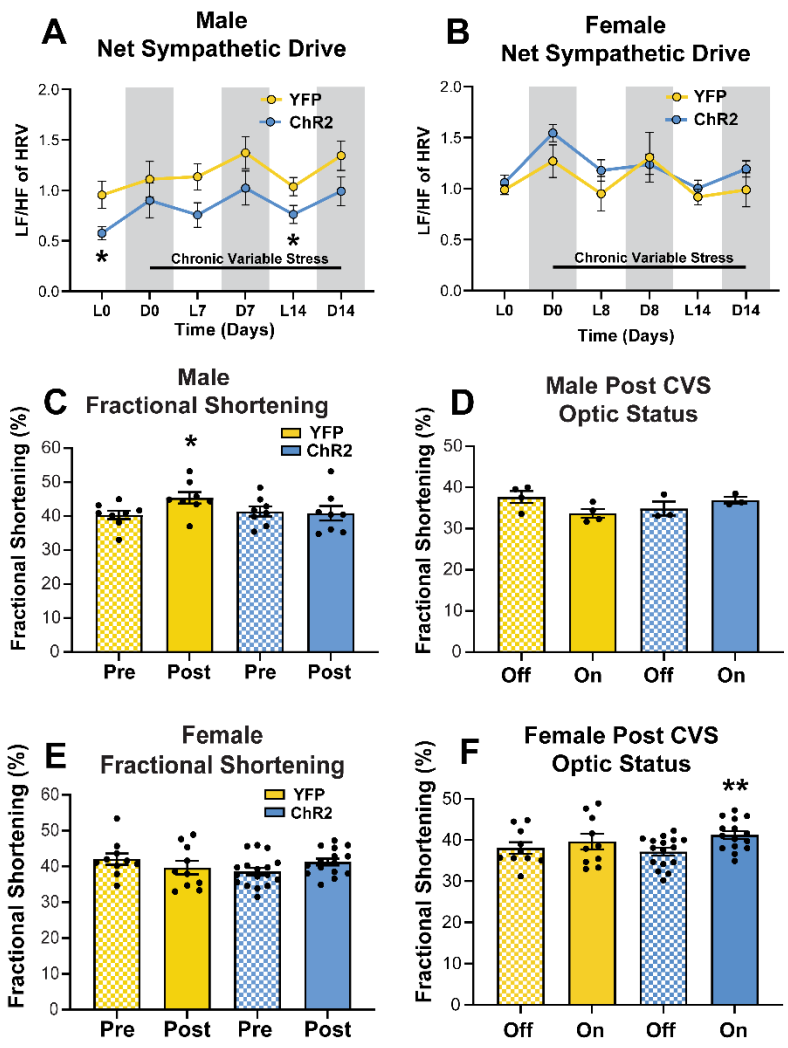

Figure 6: The effects of chronic stress and IL activity on cardiac function. (A) The ratio of LF to HF components of HRV were reduced in ChR2 males at baseline and the end of CVS. **(B)** Females had no treatment-based effects on net sympathetic drive. L: light phase, D: dark phase, LF: low frequency, HF: high frequency, HRV: heart rate variability. **(C)** CVS increased FS in YFP but not ChR2 males. **(D)** Acute optic status (On vs. Off) did not affect FS in males. **(E)** Females showed no changes in FS after CVS. **(F)** However, acute optogenetic activation increased female FS after CVS. * $p < 0.05$ vs YFP or Pre CVS YFP, ** $p < 0.01$ vs. ChR2 Off.

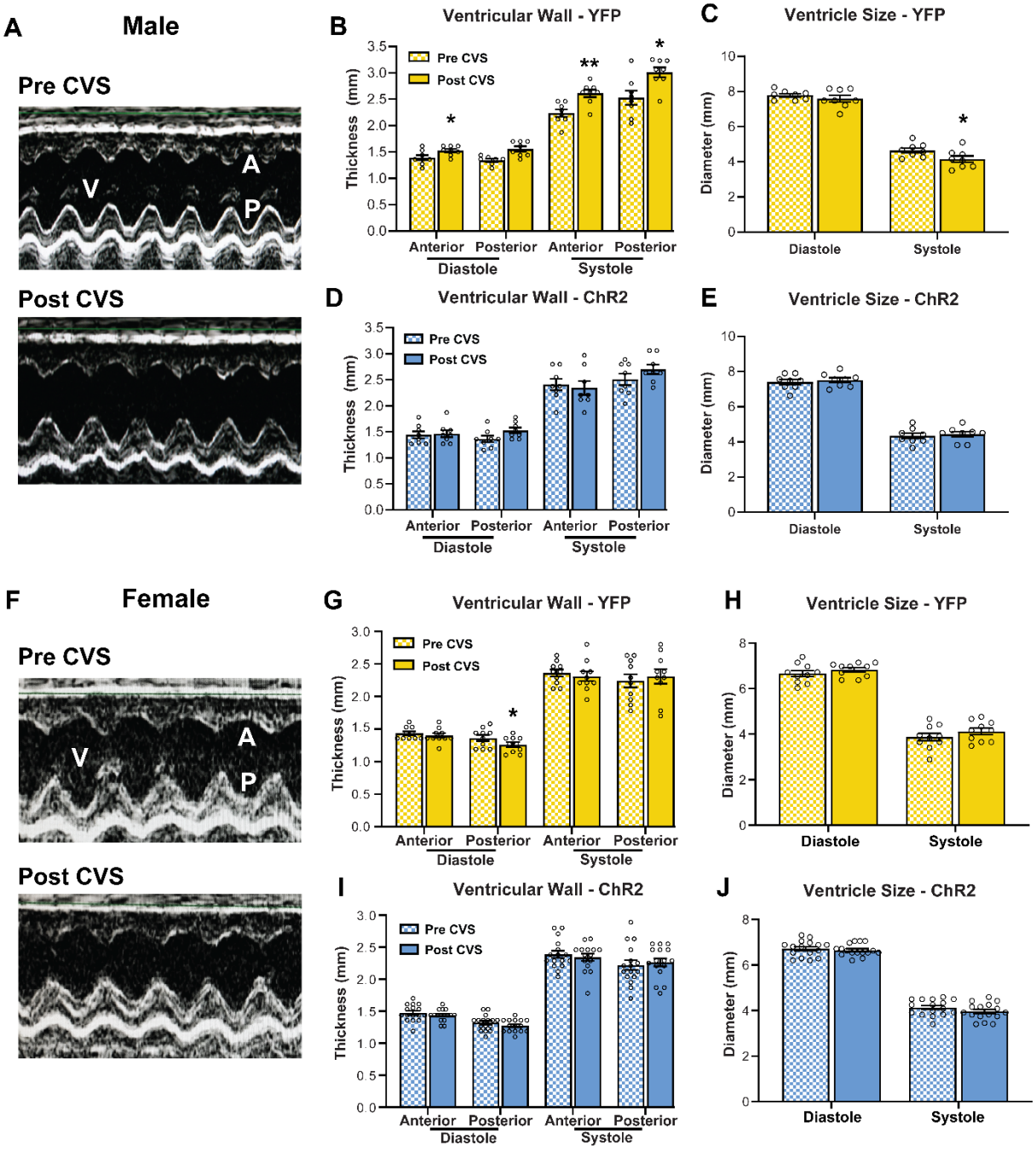

Figure 7: Effects of chronic stress and prior IL stimulation on cardiac structure. **(A)** Representative echocardiographic images of the left ventricle in bisected m-mode view before and after CVS in YFP males. V: ventricle, A: anterior wall, P: posterior wall. **(B)** CVS increased wall thickness in diastole and systole in YFP males, **(C)** reducing ventricle size. **(D, E)** ChR2 males that received prior stimulation were protected from the cardiac consequences of CVS. **(F)** Representative m-mode view of the left ventricle in YFP females before and after CVS. **(G, H)** Females did not exhibit ventricular hypertrophy after CVS as posterior wall thickness in diastole was decreased. **(I, J)** No

myocardial structural changes were evident in ChR2 females. n = 8-16/group, * $p < 0.05$, ** $p < 0.01$ vs. Pre CVS YFP